Available online at www.sciencedirect.com
SCIENCE DIRECT®
International Journal of Heat and Fluid Flow 24 (2003) 835–852
International Journal of HEAT AND FLUID FLOW
www.elsevier.com/locate/ijhff

Non-linear dynamics and pattern formation in a vertical fluid layer heated from the side

Dmitry A. Bratsun *, Alexej V. Zyuzgin, Gennady F. Putin

Perm State University, 15, Bukirev St., 614600 Perm, Russia

Received 9 September 2002; accepted 22 May 2003

Abstract

We study both experimentally and numerically the convective flow in a tall vertical slot with differently heated walls. The flow is investigated for the fluid with the Prandtl number $Pr = 26$, which is large enough to ensure the traveling waves as primary instability and small enough to prevent boundary layer convection. The flow evolution is determined on the base of the visual observations, power spectra and amplitude analysis. In the numerical simulations of two- and three-dimensional flows, we accept an assumption of an infinite fluid layer. The satisfactory agreement with experiment is observed, and the sequence of convection states is discovered. It starts with a plane-parallel flow as primary solution, which becomes unstable to two counter-propagating waves. It is followed by a tertiary three-dimensional flow in the form of wavy traveling waves. As the Grashof number is increased even further, a chaotically oscillating cellular pattern consisting of the pieces of broken waves arises. The formation of a structure in the form of the vertical rolls chaotically modulated along axes concludes this complicated picture.

Keywords: Thermal convection; Vertical layer; Pattern formation; Transition to chaos; Traveling-wave instability

1. Introduction

Since pioneering works by Gershuni (1953) and Batchelor (1954) the problem which deals with the natural convection in a slot with a fixed temperature difference between the vertical side walls continues to attract the attention of researchers because of its considerable scientific and engineering importance.

As it is known, in a vertical rectangular slot differently heated from the side walls there are buoyancy forces that result in the convective flow: the fluid rises along the hot wall and comes down along the cold one. When the slot is of infinite vertical extent that is quite often assumed in theoretical considerations, the flow is parallel. This is also true in the case of finite, but sufficiently tall slot away from the top and bottom ends. In this regime, vertical velocity profile is a cubic polynomial, the temperature distribution is linear and the heat is transferred across the slot by conduction.

A lot of previous works of different authors have been devoted to the study of the instabilities associated with this conduction regime. It was shown that the type of instability is determined by the magnitude of the Prandtl number. The critical disturbance modes are hydrodynamically driven and stationary when $Pr < 12.45$ (Birikh, 1966), but they are thermally driven and oscillatory when $Pr > 12.45$ (Birikh et al., 1972; Korpela et al., 1973). Non-linear analysis has shown that former disturbances evolve into a pattern of steady transverse rolls (Gershuni et al., 1968), and the latter ones cause the convection in the form of two counter-propagating waves, one of which travels up on the warm side of the layer and another travels down on the cold side (Gershuni et al., 1974). For a highly accurate determination of this important value of Pr see the paper of Fujimura and Mizushima (1991).

One of the most interesting aspects of natural convection is the occurrence of secondary, tertiary and other supercritical motions in the process of the transition from laminar to turbulent fluid flow. The non-linear evolution of instabilities of a plane-parallel flow of

* Corresponding author. Address: Center for Nonlinear Phenomena and Complex Systems, Service Chimie Physique, CP231, Université Libre de Bruxelles, B-1050 Bruxelles, Belgium. Tel.: +32-02-650-57-81; fax: +32-02-650-57-67.

E-mail address: dbratsun@ulb.ac.be (D.A. Bratsun).

0142-727X/$ - see front matter © 2003 Elsevier Inc. All rights reserved.
doi:10.1016/S0142-727X(03)00086-9

Nomenclature

c	phase velocity of wave
F	frequency of oscillations
g	acceleration due to gravity
Gr	Grashof number, $g\beta\Theta h^3/\nu^2$
H	height of cavity
h	half-depth of cavity
k_i	wave number in i-direction
$\mathbf{n}$	unit vector in x-direction
Nu	Nusselt number
p	pressure
Pr	Prandtl number, ν/χ
S_i	generators of symmetry
t	time
T	temperature
T_b	temperature profile for base flow
v_i	velocity components
$\mathbf{v_b}$	velocity profile for base flow
x, y, z	spatial coordinates
Δx	mesh size
Greeks	
γ	unit vector in vertical direction
Δ	aspect ratio, $H/2h$
χ	thermal diffusivity
λ	increment of instability
ν	kinematic viscosity
ρ	density
σ_i	singular values
Θ	temperature difference
Ψ	stream function
Φ	vorticity

low-Prandtl-number fluid in a differently heated vertical layer was intensively studied both theoretically and experimentally, and seems to be well established (see, for example, papers by Gershuni et al. (1968), Hart (1971), Lee and Korpela (1983), Nagata and Busse (1983), Clever and Busse (1995)).

In contrast with this, the situation regarding the evolution of the traveling-wave structures, which occur at $Pr > 12.45$, is not so satisfactory. One of the phenomena that have been studied primarily from the experimental (Elder, 1965 ($Pr = 1000$); Seki et al., 1978 ($Pr = 480$); Chen and Wu, 1993 ($Pr = 720$); Wakitani, 1994 ($Pr = 900$); Chen and Thangam, 1985 ($Pr = 158$–720)), analytical (Korpela et al., 1973; Bergholz, 1978) and numerical (Jin and Chen, 1996 ($Pr = 158$–720); Christov and Homsy, 2001 ($Pr = 1000$)) point of view is a pattern formation in high-Prandtl-number fluids. It is important to notice however, that for so high values of the Prandtl number as above, fluid inertia becomes insignificant and only thermal inertia plays a role. It means that the heat is rather convected than diffuses. This causes an accumulation of heat in the upper part of the slot and even onset of stationary secondary flow instead of traveling waves (Elder, 1965; Bergholz, 1978). Thus, if one intends to study the evolution of traveling waves pattern, one should look at moderate-Prandtl-number fluids. It was surprising for us, but we could find only a few works in the literature sharing this point of view.

Let us discuss some difficulties arising at the experimental study of a traveling-wave instability in the vertical layer in more detail. It is evident that the developed regime associated with such an instability can only be observed in sufficiently tall slots. The estimate for slot's height can be obtained as follows. A characteristic time required for development of disturbances may be written as $1/\lambda$, where λ is a maximal value of increment inside domain of instability (λ may be calculated from linear stability analysis). It is clear that this time must be less than those of wave travel along the slot, which may be written as H/c, where H is a height of slot and c is a phase velocity of wave. In the dimensionless form we obtain the following condition:

$$\Delta > Gr_\mathrm{cr}\frac{c}{2\lambda}, \tag{1}$$

where Gr_cr denotes the critical value of the Grashof number for the onset of instability, and $\Delta = H/2h$ is aspect ratio (h is a half-depth of slot). It should be noted that the critical Grashof number is function of the Prandtl number: $Gr_\mathrm{cr} = Gr_\mathrm{cr}(Pr)$. For example, for alcohol ($Pr = 14$) the estimate (1) gives unrealistically high value $\Delta > 1000$. This means that the secondary oscillatory flow observed typically in alcohol are "transitional" in that sense that the traveling-wave disturbances in the opposing flows have no time to grow up to a state of interaction between them. This conclusion is corroborated by the results for the slot of alcohol obtained by Kirdyashkin et al. (1971). Authors have observed the secondary convective regime in the form of two series of transverse rolls, one of which rises along the hot wall and another comes down along the cold one.

On the other side, the theoretical assumption that a layer has an infinite vertical extent implies evidently the interaction between the opposing streams. In fact, the numerical modeling of the two-dimensional convective flows in an infinite layer performed by Gershuni et al. (1974) for $Pr = 16$ has predicted the structure which is quite different from those observed experimentally. According to their results, the flow pattern consists of transverse rolls located between ascending and de-

scending streams. Intensities of neighboring rolls pulsate periodically in anti-phase. Such a disagreement between theory and experiment is clearly due to the usage in experiments of the cavities which do not satisfy (1). Note that the condition (1) becomes less strict for fluids with larger values of the Prandtl number. However, another difficulty has then appeared. In order to reach a point of instability of the conduction regime, an experimenter needs to rise the temperature difference between side walls up to the value

$$\Theta = Gr_{\mathrm{cr}} \frac{\nu^2}{g\beta h^3}, \tag{2}$$

where ν is the kinematic viscosity, β is the volumetric coefficient of thermal expansion and g is the gravitational acceleration. One can see that as the depth h is decreased, the critical temperature difference increases. By this reason one opts typically for the slots with h, which is sufficient to obtain the primary instability of the base flow: $Pr = 100$, $h = 10$ mm (Kirdyashkin et al., 1971); $Pr = 1000$, $h = 10$–50 mm (Elder, 1965); $Pr = 480$, $h = 10$ mm (Seki et al., 1978). But in a moderately high cavity, when the Grashof number is increased, the flow undergoes the transition to a boundary layer regime before the conduction state becomes unstable with respect to the oscillatory disturbances interesting for us in the present paper. In these cases, a flow with steep velocity and temperature gradients confined to boundary layers on the vertical side walls and a core in the center are usually observed. It is clear that in such a situation the opposing streams do not interact again. As the Prandtl number is increased, the heat advection in such fluids becomes more effective in comparison with thermal conduction, and the probability for boundary layer regime to take place becomes higher.

So, in order to observe experimentally the interaction and evolution of the traveling-wave disturbances in a tall vertical slot, one needs to opt for the fluid with moderate value of the Prandtl number, approximately from the range $20 < Pr < 40$. In order to satisfy this requirement, we have used kerosene, $Pr = 26$, as the working fluid. Such a choice of fluid and the usage of cavity satisfying (1) offer new opportunities for the comparison of experimental data with results obtained numerically for the layer of infinite extent.

Let us mention now the main difficulty met by researchers when natural convection in moderate-Prandtl-number fluid is studied numerically. Although the problem of the linear stability of the base flow with respect to the traveling-wave disturbances has been considered adequately (see, for example, papers by Birikh et al. (1972) and Korpela et al. (1973)), the study of nonlinear evolution of even two-dimensional disturbances has faced the following obstacle mentioned by Gershuni et al. (1974) and Lee and Korpela (1983). The amplification rate of disturbances inside of instability domain was so small and the transition time to limiting oscillatory regime was so long, that it was not possible to provide the systematic investigation of bifurcations and phase dynamics for the secondary and tertiary flows. As far as we know to date, the works devoted to the three-dimensional unsteady flows in a tall vertical slot are practically absent.

Such an uncertainty concerning the evolution of the traveling waves in the interacting opposing streams has motivated the investigation presented in this paper. As an example of such behavior, we explore both numerically and experimentally the transition from laminar to irregular convection in the layer of kerosene ($Pr = 26$). The paper is organized as follows: in Section 2 we formulate the problem. The details of numerical scheme and numerical results are presented in Section 3. Section 4 gives the details of experiment and experimental results. Having established the values of the Grashof number for the principal bifurcations, we then discuss the pattern formation in the system and provide the comparison between theory and experiment in the Section 5. Section 6 gives the summary.

2. Formulation

We will consider the motion of an incompressible fluid enclosed between two parallel vertical walls that a distance $2h$ apart. These walls are infinite in extent and located in the planes $x = -h$ and $x = h$. We will use a Cartesian system of coordinates with the origin on the median plane of the layer, where the y-axis is taken to point in the vertical direction, and the z-axis is horizontal and parallel to the walls. We will assume that there is a horizontal temperature difference of 2Θ applied across the wall with the wall at $x = -h$ being the hotter. This configuration is shown schematically in Fig. 1. The flow in such a cavity is assumed to be governed by the Boussinesq form of the Navier–Stokes equations, which are

$$\frac{\partial \mathbf{v}}{\partial t} + \mathbf{v}\cdot\nabla\mathbf{v} = -\nabla p + \Delta\mathbf{v} + Gr\,T\gamma,$$

$$\frac{\partial T}{\partial t} + \mathbf{v}\cdot\nabla T = \frac{1}{Pr}\Delta T, \quad \nabla\cdot\mathbf{v} = 0, \tag{3}$$

where γ is the unit vector in y-direction. Eq. (3) have been put into non-dimensional form by scaling length by h, time by h^2/ν, velocity by ν/h, temperature by Θ, and pressure by $\rho\nu^2/h^2$. In the above equations, there are only two independent parameters that describe the flow. These are

$$Gr = \frac{g\beta\Theta h^3}{\nu^2}, \quad Pr = \frac{\nu}{\chi},$$

the Grashof number and the Prandtl number respectively. In the present paper, the Prandtl number will be

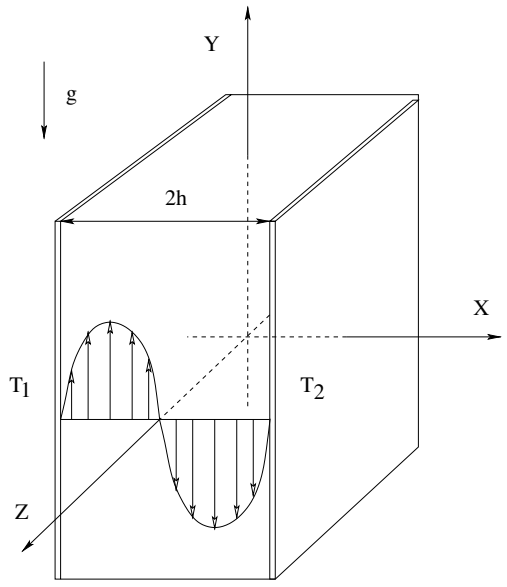

Fig. 1. Geometrical configuration of the problem.

fixed to value $Pr = 26$ corresponding to kerosene. Thus, the Grashof number is only parameter which governs the flow evolution.

The boundary conditions for the velocities are the non-slip conditions at the walls. The temperature has a value 1 at the left wall and −1 at the right wall:

$$x = \pm 1: \quad \mathbf{v} = 0, \quad T = \mp 1. \tag{4}$$

In the y- and z-directions the periodicity conditions are applied over a cell defined by the wave numbers k_y and k_z respectively:

$$\begin{aligned} \mathbf{v}(x,y,z,t) &= \mathbf{v}\left(x, y+\frac{2\pi}{k_y}, z+\frac{2\pi}{k_z}, t\right), \\ T(x,y,z,t) &= T\left(x, y+\frac{2\pi}{k_y}, z+\frac{2\pi}{k_z}, t\right). \end{aligned} \tag{5}$$

The primary solution of Eqs. (3) and (4) describing the basic state of the system is given by

$$\mathbf{v_b} : (0, v_y, 0), \quad v_y = \frac{1}{6} Gr(x^3 - x), \quad T_b = -x, \tag{6}$$

and corresponds to the flow in the conduction regime.

3. Numerical simulation

3.1. The solution method

In order to perform a non-linear simulation of the two-dimensional flows, we use a vorticity–stream function formulation of the governing equations (3). By introducing the stream function

$$v_x = \frac{\partial \Psi}{\partial y}, \quad v_y = -\frac{\partial \Psi}{\partial x},$$

the vorticity

$$\Phi = \frac{\partial v_y}{\partial x} - \frac{\partial v_x}{\partial y},$$

and eliminating the pressure, we can rewrite Eq. (3) in the following form:

$$\begin{aligned} &\Delta \Psi = -\Phi, \\ &\frac{\partial \Phi}{\partial t} + \frac{\partial(\Phi, \Psi)}{\partial(x,y)} = \Delta \Phi + Gr \frac{\partial T}{\partial x}, \\ &\frac{\partial T}{\partial t} + \frac{\partial(\Psi, T)}{\partial(x,y)} = \frac{1}{Pr} \Delta T. \end{aligned} \tag{7}$$

We solve this system of equations in the domain $-1 < x < 1$, $-H/2 < y < H/2$ with the following conditions on the boundaries:

$$\begin{aligned} &x = \pm 1: \quad \Psi = \frac{\partial \Psi}{\partial x} = 0, \quad T = \mp 1, \\ &y = \pm H/2: \quad \Psi(x, -H/2, t) = \Psi(x, H/2, t), \\ &\qquad\qquad\quad T(x, -H/2, t) = T(x, H/2, t). \end{aligned} \tag{8}$$

As the initial state we used the vorticity field characterized by one or more one-vortex structures. In all cases the numerical experiments have recovered the independence of the final state on the initial condition.

The boundary value problem (7) and (8) was solved by the finite-difference method. Equations and boundary conditions were approximated on a uniform mesh using a second order approximation for the spatial coordinates. The non-linear equations were solved using an explicit scheme on a rectangular uniform mesh 80×160 (for $H = 4$). To ensure the convergence of the numerical scheme, the time step was calculated by the formula

$$\Delta t = \frac{\Delta x^2}{2(2 + \max(|\Psi|, |\Phi|))},$$

where Δx is the mesh size. The Poisson equation was solved by the iterative Liebman successive over-relaxation method in each time step: the accuracy of the solution was fixed to 10^{-4}. The Kuskova and Chudov formulas, providing the second order accuracy, were used for approximation of the vorticities at the vertical boundaries $x = \pm 1$:

$$\Phi(-1, y) = \frac{1}{2\Delta x}(\Psi(-1 + 2\Delta x, y) - 8\Psi(-1 + \Delta x, y)),$$

$$\Phi(1, y) = \frac{1}{2\Delta x}(\Psi(1 - 2\Delta x, y) - 8\Psi(1 - \Delta x, y)).$$

To test of accuracy and convergence of our computer program we have performed calculations of the thermal convection in a square cavity heated from the side walls. In all cases, it was found that our results agree with corresponding numerical results reporting in the literature.

For the numerical simulation of spatially periodic three-dimensional flows, we have used the code "NEKTON" (the computations were carried out on 8 node Intel-iPSC/860 of IMF (Marseille, France)) employing a spectral-element method (Patera, 1984) adapted for parallel implementation on multi-processor computers by Fischer (1989). The spectral-element method is a generalized variational scheme which exploits the rapid convergence rates of spectral methods while retaining the geometric flexibility of the finite element technique. It is based upon a macro-(spectral) element discretization, where on each element the solution has a polynomial expansion of high degree. In the code "NEKTON", the Legendre polynomials are used as basis functions. The method is thus characterized by the discretization pair (K,N), where K is the number of spectral elements and N is the order of polynomial approximations. In our calculations we used the number of elements ranging from $K = 4$ in the two-dimensional case to $K = 48$ in the three-dimensional case. In all cases the order of polynomials was fixed $N = 7$.

The time advancement scheme included the explicit Adams-Bashforth treatment of the non-linear convective terms and implicit Uzawa procedure for the treatment of viscous term. The Jacobi-preconditioned conjugate-gradient iterative algorithm was used to resolve the system on each time step.

The calculations have been performed in a wide range of the wave number k_y: $0.4 \leqslant k_y \leqslant 1.1$ for two-dimensional flows and in the cell defined by $k_y = \pi/4$, $k_z = \pi/3$ for three-dimensional flows. Pulsations of the velocity and temperature have been recorded in the center of (y,z)-plane in the point $x = -0.59$.

3.2. Time-dependent two-dimensional flows

In this section we present the numerical results for two-dimensional flows assuming that each variable is a function of the x- and y-coordinates only and $\partial/\partial z = 0$, $v_z = 0$.

Stability boundaries for the different time-dependent regimes of convection in the (k_y, Gr)-parameter plane are shown in Fig. 2, where the neutral stability curve for the base flow is indicated by the solid line and the boundaries corresponding to various secondary nonlinear convective patterns, are indicated by point-lines. We have re-calculated the linear stability curve for $Pr = 26$ using the procedure described in the monograph by Gershuni and Zhukhovitskii (1976). The minimum of neutral curve is located in the point $k_{y\min} = 0.94$, $Gr_{\min} = 114.5$. The line marked by open squares corresponds to the appearance of time-periodic flow which replaces the conduction state (6). As it can be seen from Fig. 2, this curve is tangent to neutral stability curve approximately in the point of minimum. The similar result was obtained by Gershuni et al. (1974) for $Pr = 20$.

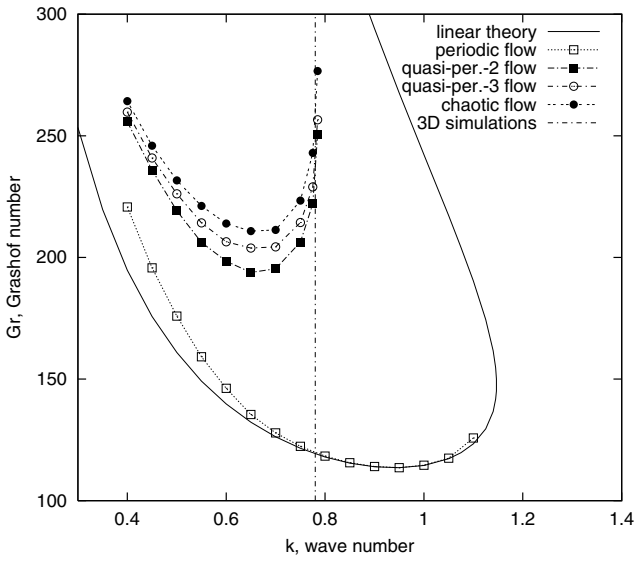

Fig. 2. Diagram of stability for two-dimensional flows.

We found that as the Grashof number Gr is increased, the system undegoes at least three Hopf bifurcations, starting from the stationary solution (6) to the chaotical behavior.

Let us discuss in more detail, for example, the bifurcation sequence for the flow with the wave number fixed to $k_y = \pi/4$ (indicated in Fig. 2 by the vertical dashed line). Some representative results including the power spectra and Poincaré maps are shown in Fig. 3(a)–(d) for $Gr = 220$, 230, 248 and 250, respectively. The Poincaré cross-section of the phase space constructed by v_x, v_y and T recorded in one point has been defined by the condition: $v_x = 0$. In fact, the x component of velocity characterizes the deviation of the secondary flow from plane-parallel one (6). We found that the first Hopf bifurcation is supercritical and occurs at about $Gr = 124$. The frequency of oscillations is found to be practically a linear function of the Grashof number, and such a relationship does not depend on wave number k_y. Near the bifurcation point, the system oscillates with the frequency $F_1 = 1.1$. As the Grashof number is increased to 220, the frequency also increases to 1.42 (Fig. 3(a)).

The stream pattern replacing the base state is a system of clockwise-rotating vortices, periodic in the vertical direction, which stand between ascending and descending flows (Fig. 4, left). Intensities of neighboring vortices are changed periodically in anti-phase. In contrast with the standing pattern shown by streamlines, the temperature field is a pair of traveling waves, one of which propagates along the hot wall upward and another propagates along the cold wall downward (Fig. 4, right). That is why this regime is called sometimes as "temperature waves". It should be noted that the similar structure has been obtained numerically by

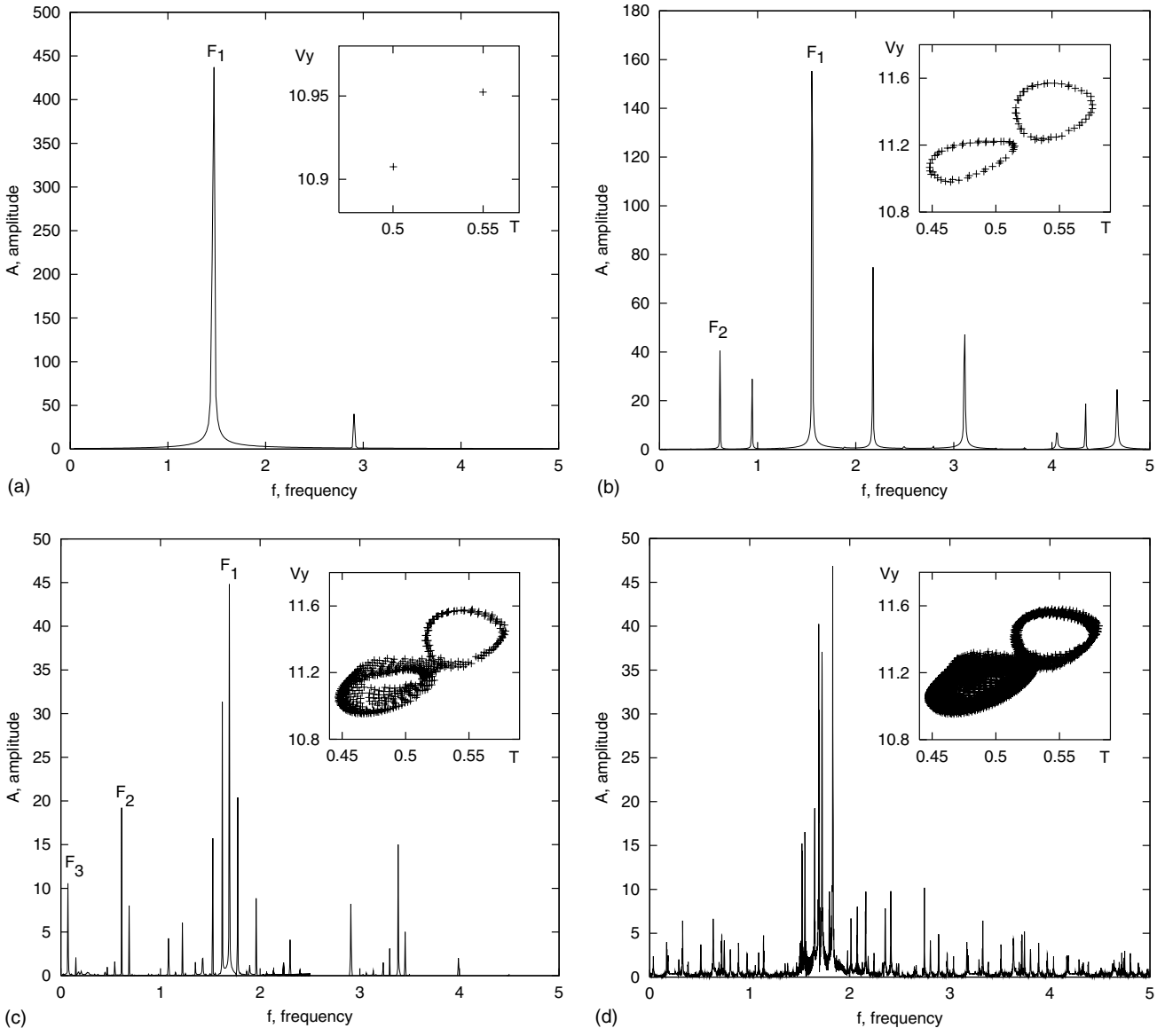

Fig. 3. The power spectra and Poincaré maps for two-dimensional time-dependent flows: (a) $Gr = 220$, periodic behavior; (b) $Gr = 230$, two-frequency quasi-periodic behavior; (c) $Gr = 248$, three-frequency quasi-periodic behavior; (d) $Gr = 250$, chaotic behavior. The Poincaré cross-section has been defined by the condition: $v_x = 0$.

Gershuni et al. (1974) for $Pr = 20$ and Chait and Korpela (1989) for $Pr = 1000$.

We have found that an increase of Gr further leads to sequential bifurcations: first, to the torus of dimension two characterized by the two incommensurate frequencies: $F_1 = 1.48$, $F_2 = 0.65$ at $Gr = 230$ (Fig. 3(b)), and then to the torus of dimension three with the frequencies: $F_1 = 1.69$, $F_2 = 0.61$, $F_3 = 0.07$ at $Gr = 248$ (Fig. 3(c)).

In our calculations we have obtained the solutions with as many as four fundamental incommensurate frequencies, and quite possible that there could exist the oscillations characterized by even more frequencies, but, due to the numerical difficulty mentioned in introduction, the registration and study of such quasi-periodic solutions are not easy. For example, in order to obtain the limit cycle at $Gr = 130$ one need to integrate the system during about $t_{\text{num}} \approx 70\tau$, where τ is the period of oscillations. For the two-frequency quasi-periodic solution at $Gr = 230$ the integration takes already $t_{\text{num}} \approx 600\tau$. Finally, the three-frequency quasi-periodic state at $Gr = 248$ demands as much time as $t_{\text{num}} \approx 2800\tau$!

It is interesting to note that the described transition of the system through several quasi-periodic state can be explained in the physical terms. The basic frequency F_1 is naturally associated with a speed of the temperature waves arising due to the primary oscillatory instability. As for other frequencies, which are usually a smaller

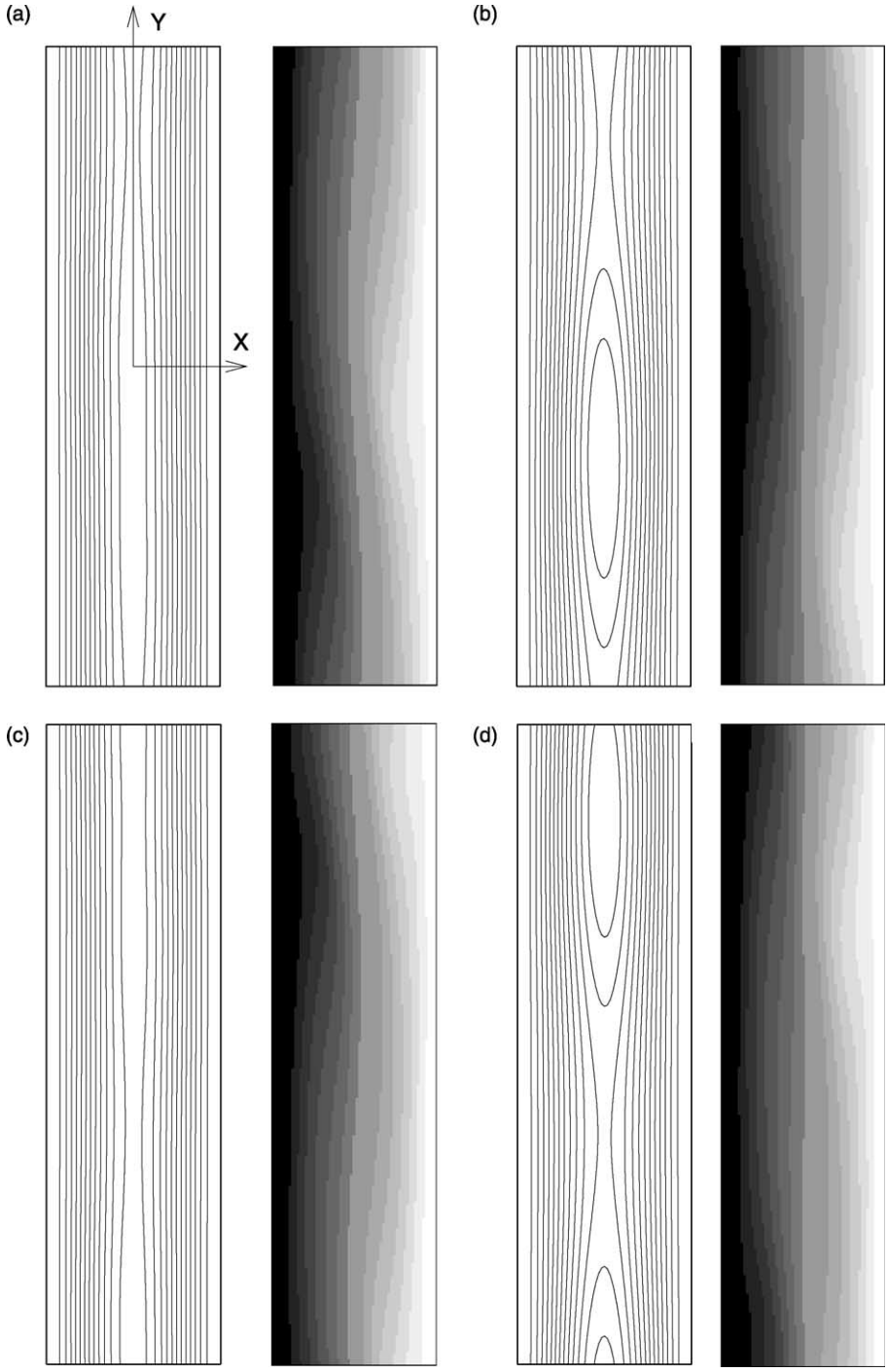

Fig. 4. Streamlines (left) and isotherms (right) for the oscillatory two-dimensional convective pattern ($k_y = \pi/4$) are shown in the cycle of periodic state at $Gr = 150$: (a) $t = 0$; (b) $t = \tau/4$; (c) $t = \tau/2$; (d) $t = 3\tau/4$, where τ is the period of oscillations.

value, its origin is not so evident. In our opinion, an addition of new fundamental frequencies occurs due to a modulation of the temperature waves. The analysis of animation of pattern isotherms during the quasi-periodic regime has shown that the process of new frequency appearance takes place as follows. As the Grashof number is increased, the amplitudes of opposing hot and cold temperature waves grow up to moment when one wave begins to overlap over another. We have found that value of Gr, when it happens, corresponds approximately to the bifurcation to quasi-periodic solution. The explanation is quite simple. Due to the different temperatures of waves, one wave slips over another. This interaction gives rise to the additional disturbances modulating the amplitude of each wave. As we mentioned already, the relaxation time for the

thermal disturbances in a high-Prandtl fluid is comparatively large, and thermal disturbances are convected by flow rather than disappear due to conduction. This leads to the appearance of the new fundamental frequency F_2 and complicates flow pattern. Thus, this modulated state may be characterized as two wave—the original temperature wave and its modulation—traveling at independent rates. We found that the frequencies F_1 and F_2 do not lock as Gr varies, even when they pass through small rational numbers. Further appearance of new independent frequencies may be explained in the similar manner.

The curve marked in Fig. 2 by black circles indicates the onset of chaotic oscillations in the system. We found that the transition to chaos occurs via destruction of a high-dimensional torus (dimension three, or even more—depending on the wave number k_y) and appearance of a strange attractor. The power spectum and Poincaré map for one of a such solution is shown in Fig. 3(d).

As it is known, a non-linear dynamical system with chaotic behavior exhibit a number well established routes to chaotic behavior. Starting with the pioneering work of Ruelle and Takens (1971), a lot of effort has been devoted to study transitions to chaos through quasi-periodic motion. The most general transition of this kind usually proceeds from two-frequency quasi-periodic behavior to low-dimensional chaotic motion through the interaction of resonances (mode-locking), that lead to a corrugation of the torus, and ultimately to a strange attractor. The very existence of three-dimensional tori within this scenario appears unlikely in the light of the Ruelle–Takens theorem. However, both experiments and numerical studies give support to the existence of these attractors insisting that in some cases they can be structurally stable. For example, experimentally three-frequency quasi-periodic motion has been documented by Gollub and Benson (1980), and four-frequency and five-frequency quasi-periodic motion by Walden et al. (1984). Some further light has been shed on this topic after the work of Feudel et al. (1993), who have presented convincing arguments on the stability of three-dimensional tori on systems with certain types of symmetries, when the perturbations that affect these attractors are not generic due to the symmetry of the system. Two of the reported routes that involves a 3D-torus are:

2D-Torus → 3D-Torus → 2D-Torus → Chaos (Feudel et al., 1993),
2D-Torus → 3D-Torus → High-dimensional chaos (Pazó et al., 2001).

Thus, our results may be consistent with one of these scenarios predicting that non-periodic motion should occur after a small number of quasi-periodic bifurcations.

3.3. Time-dependent three-dimensional flows

As it is known from numerous experiments (Elder, 1965; Kirdyashkin et al., 1971; Seki et al., 1978), when the Grashof number is increased, the convective flow in vertical slot becomes unstable with respect to the three-dimensional disturbances.

In order to study the flow pattern which arises as a result of development of such disturbances, we have performed the simulation of spatially periodic three-dimensional flows in a cell defined by $-1 < x < 1$, $-4 < y < 4$, $-3 < z < 3$, which corresponds to wave numbers $k_y = \pi/4$, $k_z = \pi/3$.

In order to characterize a heat transfer in the cell, we define the Nusselt number as the ratio of actual heat transport across the layer to the heat transported only by conduction, and average it over time:

$$Nu = \frac{1}{\tau}\int_0^\tau \frac{\int \mathbf{n}\cdot\nabla T\,\mathrm{d}y\,\mathrm{d}z}{\int \mathbf{n}\cdot\nabla T_\mathrm{b}\,\mathrm{d}y\,\mathrm{d}z}\mathrm{d}t,$$

where $\mathbf{n}$ is the unit vector in x-direction and τ is sufficiently long period of time.

First, let us discuss the situation in the range of the Grashof number where two- and three-dimensional flows compete against each other. Fig. 5(a) presents the variation of the Nusselt number Nu versus the Grashof number Gr. As it can be seen from figure, the two-dimensional flows provide the maximal rate of heat transfer across the layer in the range $124 < Gr < 133$. We have found that in this range of Gr, the three-dimensional disturbances being inserted in system leads always to the two-dimensional solution. But if the Grashof number exceeds the critical value, $Gr = 133$, the transverse rolls (or the traveling waves if to refer to the temperature field) shown in Fig. 4 become wavy in the z-direction. The new flow provides maximal rate of heat transfer for $Gr > 133$. The described picture is supported by the comparison of the v_x and v_z components of velocity as a function of the Grashof number Gr shown in Fig. 5(b).

We found that as the Grashof number is increased further in small steps, the transition of the three-dimensional flow to chaotic behavior in time proceeds through, first, the cycle pitchfork bifurcation which breaks symmetry and gives rise to the periodic state at $Gr = 133$, then the secondary Hopf bifurcation at about $Gr \approx 134$, which leads to the quasi-periodic motion with two independent frequencies, and ultimately to the corrugation of the torus and the strange attractor at $Gr \approx 142$. Some representative results including the power spectra, Poincaré maps and time series for the three-dimensional time-dependent flows are shown in Fig. 6(a) and (b) for $Gr = 135$ and 150, respectively. The Poincaré cross-section of the phase space (v_z, v_y, T) has been defined by the condition: $v_z = 0$. In fact, the z

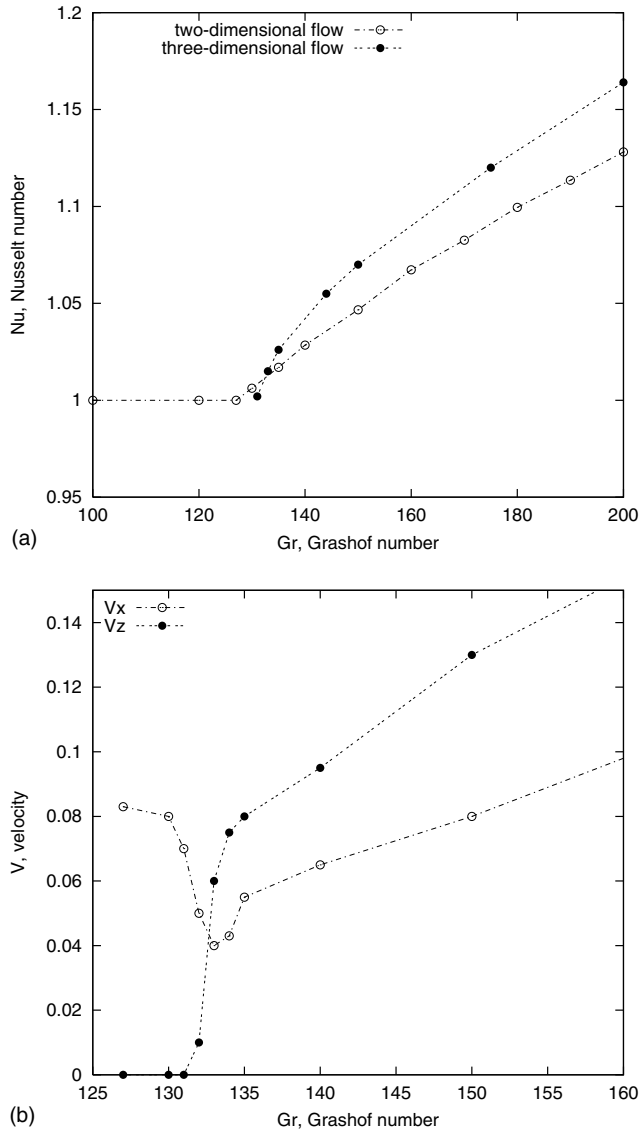

Fig. 5. Competition between the two-dimensional and three-dimensional flows. (a) The heat transport across the layer with $k_y = \pi/4$, $k_z = \pi/3$ averaged over time versus the Grashof number Gr. (b) The maximal velocities v_x and v_z averaged over time versus the Grashof number Gr.

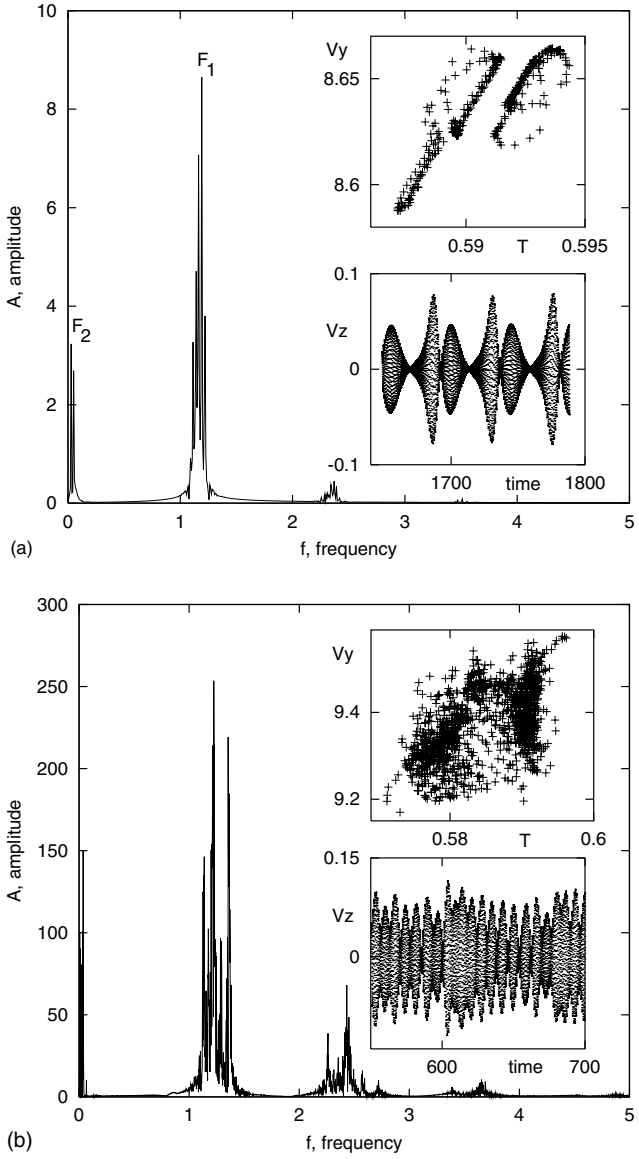

Fig. 6. The power spectra, Poincaré maps and time series for time-dependent three-dimensional flows: (a) $Gr = 135$, two-frequency quasi-periodic behavior; (b) $Gr = 150$, chaotic behavior. The Poincaré cross-section has been defined by the condition: $v_z = 0$.

component of velocity characterizes the deviation of the flow from the two-dimensional one.

It should be noted that after the pitchfork bifurcation at $Gr = 133$ there are two attractors (cycles, tori or strange attractors) in the phase space of the system. These attractors are symmetric with respect to the plane $v_z = 0$ and may be obtained one from another by applying the transformation of symmetry. It is interesting to point out that the plot of the power spectrum in Fig. 6(a) indicates the existence of sub-harmonic peaks that implies the earlier sub-harmonic bifurcation of tori.

Variation of the principal frequency F_1, which is related with a speed of the temperature waves, with the Grashof number Gr is shown in Fig. 9, where line corresponding to three-dimensional regime of convection is drawn in dashed style. Due to growing irregularity of oscillations with an increase of Gr, the principal frequency has been determined by maximum peak in the corresponding power spectra. We see that in the vicinity of bifurcation point, the results are close to those for two-dimensional flows. But as the Grashof number Gr is increased, the dashed line deviates more and more from the solid one. Thus, the growth of the three-dimensional effects in flow causes an increase of basic frequency of oscillations. By other words, the temperature waves move faster as the flow becomes more and more three-dimensional.

Thus, we see that the flow stays two-dimensional up to $Gr \approx 133$, but for higher values of the Grashof number the consideration of three-dimensional flows becomes necessary. It should be noted, that in contrast to two-dimensional convection, the three-dimensional flow undergoes the transition to temporal chaos at smaller value of Gr. In fact, our numerical simulations predict that the flow will remain regular (i.e. periodic or quasi-periodic) in the limited range of parameter: $127 < Gr < 142$. Similarly to the two-dimensional case, the transition to chaos occurs via the breakdown of quasi-periodic solution, but we have documented only the torus with two independent frequencies (Fig. 6(a)).

Let us discuss now the evolution of flow pattern. Fig. 7(a)–(d) presents the lines of constant x-component of velocity normal to the plane $x = 0.1$ in a some fixed moment of time for $Gr = 130$, 135, 150 and 300,

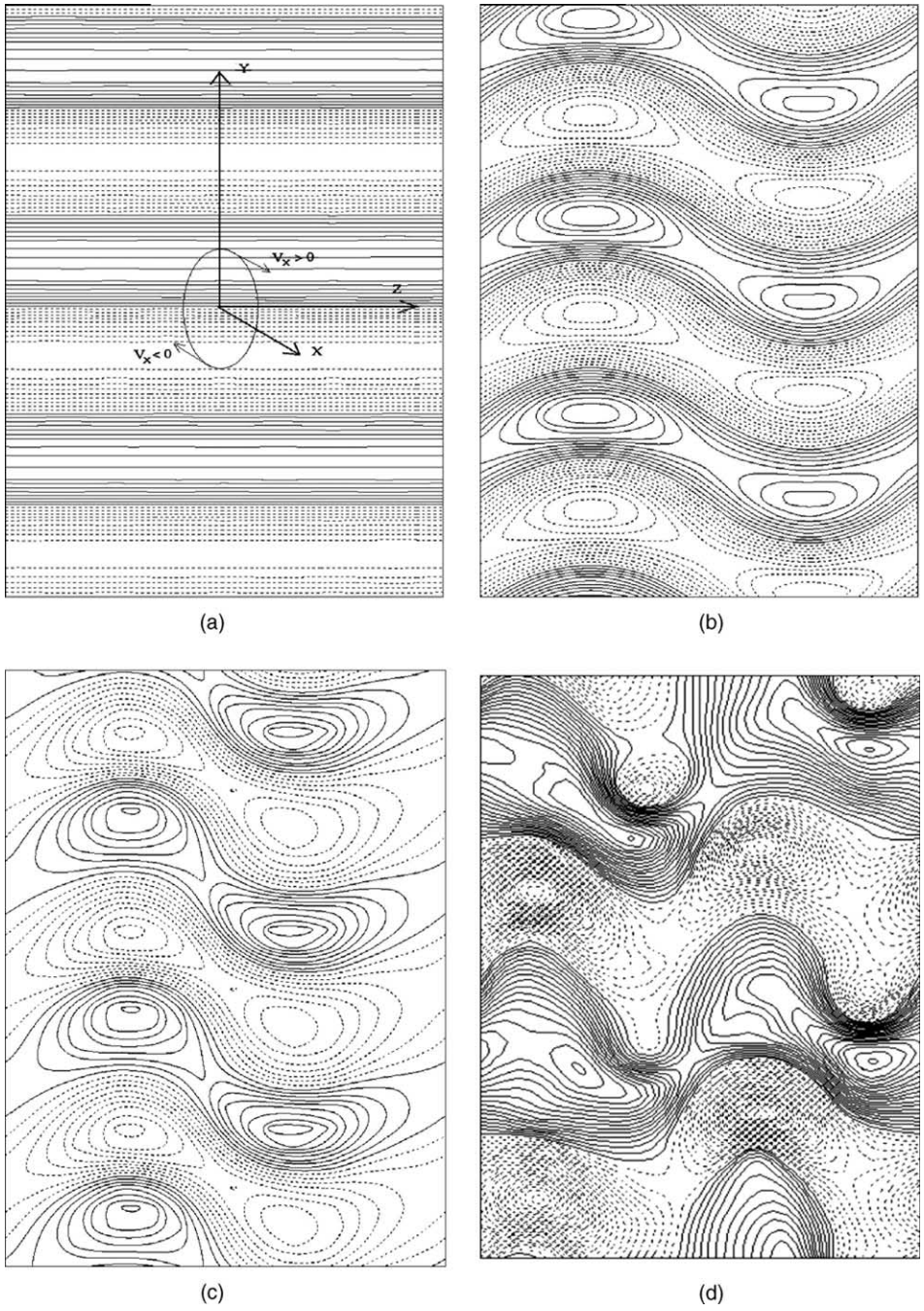

Fig. 7. Unsteady three-dimensional convection pattern. Lines of constant normal velocity, $v_x = \text{const.}$, in the plane $x = 0.1$ are shown in some fixed moment of time: (a) $Gr = 130$; (b) $Gr = 135$; (c) $Gr = 150$; (d) $Gr = 300$. Each pattern drifts as a whole structure in the negative y-direction with the constant phase velocity. Solid (dashed) lines indicate positive (negative) values. The solid line adjacent to the dashed ones indicates zero.

Table 1
Bifurcation values for main flow patterns

Convective flow pattern	Linear stability analysis, $Gr \times 10^{-2}$	Numerical results, $Gr \times 10^{-2}$	Experiment, $Gr \times 10^{-2}$		
			$\Delta = 50$	$\Delta = 75$	SVD ($\Delta = 75$)
Pulsating transverse rolls	1.18 (for $k_y = 0.79$) 1.15 ($k_y = 0.94$)	1.24 ($k_y = 0.79$) 1.15 ($k_y = 0.94$)	1.1	1.2	–
Wavy pulsating transverse rolls	–	1.33 ($k_y = 0.79$)	1.25	1.4	1.3
Cellular pattern (broken rolls)	–	–	1.45	1.55	–
Modulated vertical rolls	–	–	1.6	1.7	1.7

respectively. The negative (positive) values of v_x and v_y are indicated by the dashed (solid) lines. It should be noted that each pattern shown in Fig. 7 drifts as a whole structure in the negative y-direction with constant phase velocity. This drift can be explained by the periodic pulsation of the neighboring vortices in anti-phase. The phase velocity of the drift is equal to zero only for the plane $x = 0$, but it becomes negative for any cross-section $x > 0$ (in a colder part of the layer) and positive for $x < 0$ (in a hotter part of the layer).

We see that the pattern shown in Fig. 7(a) for $Gr = 130$ corresponds to the two-dimensional transverse rolls (also shown in x–y plane in Fig. 4). The next pattern (Fig. 7(b)) illustrates flow at $Gr = 135$, where the rolls have already become wavy. As the Grashof number is increased further, the three-dimensional effects strengthen, the rolls bend more and more and, ultimately pull apart giving rise to the cellular-like pattern (Fig. 7(c), $Gr = 150$). Sequentially, the development of the latter flow pattern leads to the structure which we have called as "modulated vertical rolls (streams)" (Fig. 7(d), $Gr = 300$). Its existence becomes more evident after the observation of flow animation, only one frame of which is shown in figure. We found that the vertical streams are composed of the pieces of pulled apart horizontal rolls. These pieces move in flow downward (or upward) and coalesce into longitudinal rolls.

Thus, our analysis of flow evolution has revealed four main patterns listed in Table 1. They are two-dimensional transverse rolls pulsating in time, the same rolls becoming wavy, the broken rolls (or cellular pattern) and the vertical rolls modulated along axes. It is important to outline, that non-linear dynamics of flow in time becomes irregular already for the wavy rolls and follows generally the Ruelle–Takens' route to the chaos. We will return to the system pattern formation in more detail in Section 5, where the comparison with experiment will be given.

4. Experiment

4.1. Apparatus and observation techniques

The convection cell, where flows were established, is a rectangular cavity 300 mm high, 80 mm wide and of variable depth (see Fig. 8, where it is indicated as 1). The cavity is confined by two heat-exchangers, one of which (2) consists of aluminum plates and another (3) is prepared from Plexiglas. The temperature difference between the side walls can reach 20 °C allowing to study the flow up to $Gr \approx 400$. It is maintained by pumping water from two thermostatic units, T_1 and T_2, through thermo-isolated tubes and heat-exchangers (2–3), and is held constant to within ±0.05 °C or better during one experiment. The heat-exchangers are separated by narrow Plexiglas frame (4) of variable depth (4 or 6 mm). Thus, the aspect ratio Δ defined in Section 1 takes on values 75 or 50 respectively. These values of Δ are large enough in order to observe in kerosene the convective motions with a strong interaction of opposing flows. We found that in the case of kerosene, the aspect ratio Δ should be more than 50 (see the condition (1)). As a working fluid we have used kerosene with the following set of the physical parameters: $\nu = 1.82 \times 10^{-6}$ m^2/s, $\chi = 0.701 \times 10^{-7}$ m^2/s, $\beta = 0.955 \times 10^{-3}$ 1/K at 20 °C.

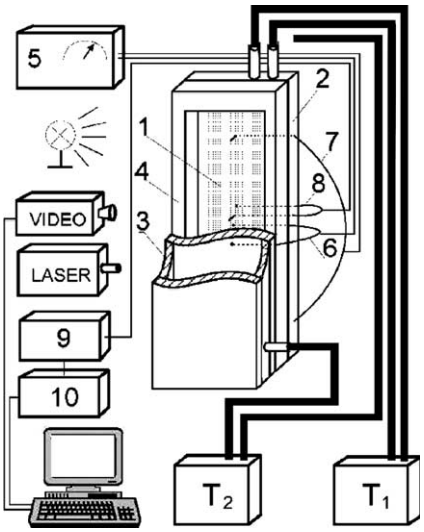

Fig. 8. Schematic diagram of experimental setup.

In order to perform the visual observations of flow patterns both in the x–y and y–z planes, one of the heat exchanger (2) was prepared from aluminum and was coloured black from the fluid side. Another heat

exchanger (3) and frame (4) were prepared from Plexiglas and was transparent. To visualize the flow, aluminum powder was suspended in the fluid. The aluminum particles are disk-shaped and tend to lie with the plane of the disk on the stream surface. This was a very helpful point because the broad features of flows were immediately apparent. Usage of aluminum powder allowed both to observe the average properties of the flow and to trace the passage of a single particle. The test experiments have shown that an addition of particles to the flow varies the critical value for onset of primary instability within ±3%. To discover the structure of flow carrying the aluminum particles, two kinds of light conditions were used: scattered light and the method of so-called "lighting knife" based on optical scheme with laser beam. The entire setup was mounted on the stable optical bench. Images of flows were acquired with a digital video camera connected to a microcomputer.

Temperatures were measured with copper-constantan thermocouples connected to a digital potentiometer (5) with fluctuation within ±0.03 °C. The temperature difference between the side walls was measured by a probe (6) located halfway between the ends of the convection cell. The vertical temperature gradient was carefully controlled by a probe (7) with the thermocouple ends, one of which was 250 mm distant from another, and with 1.5 mm of the wires inserted into cavity. In all experiments the horizontal temperature gradient was about 10^2 as large as the vertical one, ensuring that a secondary instability due to vertical temperature gradient could not occur.

In order to obtain the amplitude characteristics and frequencies of oscillatory convection regimes, we used constantan-manganin differential thermocouple (8), of which one end of diameter 0.1 mm was inserted into the flow in the middle part of the cavity at a distance of one quarter of entire cell depth and another end was located inside isothermal aluminum plate. The signal of this thermocouple was reinforced by the amplifier (9) and processed using a digital potentiometer (10) to digital conversion circuitry and then recorded by microcomputer. This equipment made it possible to measure the temperature pulsations better than ±0.003 °C. The noise level did not exceed 10^{-4} °C. The maximal frequency of oscillations which could be measured by this equipment was 18 Hz.

Several basic techniques were employed to determine the stability boundary of convection patterns. The first technique was a direct observation by continuous monitoring of space–time diagrams. The second technique was a derivation of the amplitude characteristics of the flow for each fixed value of the Grashof number. The thermocouple (8) connected to microcomputer produced a signal, which represented the pulsation of temperature field. The amplitude of these pulsations was averaged over time, and sharp change of averaged amplitude was treated as a bifurcation point for new flow pattern. In order to consider the dynamic features of the system and to check the determined stability boundaries, we performed also the technique of phase portrait reconstruction including the method of delays (Packard et al., 1980) with preprocessing using the singular value method proposed by Broomhead and King (1986). As it is known, most observational data reflect just a few of the many physical variables of a system and measurements of all variables are rarely possible. However, this difficulty can be overcome if the variables are non-linearly coupled, in which case the time-delay embedding technique proposed by Packard et al. (1980) can be used to reconstruct the phase or state space from the time series data. In this technique a multi-dimensional embedding space is constructed from the time series data, and a point in it represents the state of the system at a given time. The m-component state vector from a time series $x(t)$ can be constructed as $X_i = \{x_1(t_i), x_2(t_i), \ldots, x_m(t_i)\}$ where $x_k(t_i) = x(t_i + (k-1)\tau)$ and τ is an appropriate time delay. The reconstruction of the phase space from the time series data can yield the dynamical features in the original system, as provided by Takens' theorem (Takens, 1981).

The phase space reconstructed by time-delay embedding is noisy, and the singular spectrum analysis (Broomhead and King, 1986) can be used to remove the noise significantly. In this technique the m-dimensional state vectors X_i are used to construct a trajectory matrix X whose rows are the N vectors X_i's. This $N \times m$ matrix has all the dynamical features in the data and can be used to obtain the number of linearly independent vectors that describe the dynamics. The number of such vectors is obtained from a singular spectrum analysis of the $m \times m$ covariance matrix $X^{\mathrm{T}}X$. The number of maximal eigenvalues σ_i $(i = 1, \ldots m)$ of this matrix (frequently called as "singular values") gives an estimate of the number of variables and the eigenvectors give the directions of the variables in the embedded space. The oscillations of the system in all other directions may be treated as noise, and can be neglected. Thus, the use of singular value decomposition (SVD) allows to calculate an optimal basis for the projection of the reconstructed phase dynamics of system and decreases an influence of noise in experimental data. This technique permits an upper limit of the embedding dimension of attractor. It is evident that sharp change of attractor dimension, which manifests itself in an increase of the number of the singular values σ_i defining non-noisy phase space, with an increase of some governing parameter indicate the appearance of new convective state, i.e. system's bifurcation.

The described experimental apparatus and methods of observation and measurement allowed to define the stability boundary for different convection pattern within the error 10%. In this estimate we have taken into

account possible influences of thermal inhomogeneity of the boundaries (aluminum—Plexiglas), the vertical gradient of temperature (existing because the slot is not actually of infinite vertical dimension), the effect of dependence of viscosity on the temperature and so on.

4.2. Experimental results

In this section we present the experimental results of determination of parameter values for the principal bifurcations which occur in the system, by avoiding at the moment the detailed discussion of the system pattern formation.

The variation of amplitude of oscillations A with the Grashof number Gr is shown in Fig. 9. The values of A have been averaged over time and non-dimensionalized using half of temperature difference between side walls. The black and open squares in the figure represent the results obtained for layers with $\Delta = 50$ and 75 respectively. The squares at small values of Gr corresponds to the base stationary flow, and small deviations of experimental data from zero can be explained by a noise which always exists in system.

We have found that the secondary flow is periodic in time and space and arises at about $Gr = 1.1 \times 10^2$ for $\Delta = 50$ and $Gr = 1.2 \times 10^2$ for $\Delta = 75$. The bifurcation point has been determined by extrapolating the amplitude curves up to the point of intersection with the axis $A = 0$. The critical values of Gr derived by this way are given in Table 1. When it was not possible to determine the onset of new convection state from amplitude characteristics we have obtained the critical values from visual observations.

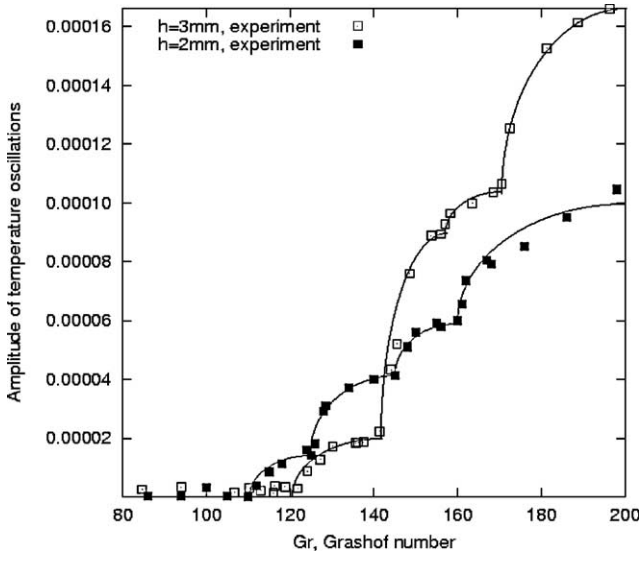

Fig. 9. The variation of dimensionless amplitude of oscillations averaged over time with the Grashof number. Black and open squares represent the results for $\Delta = 50$ and 75 respectively.

The visual observations have shown that the secondary flow remains two-dimensional only for the Grashof numbers slightly exceeding the point of the onset of oscillations. As Gr is increased further, the new pattern has been detected at about $Gr = 1.25 \times 10^2$ for $\Delta = 50$ and $Gr = 1.4 \times 10^2$ for $\Delta = 75$. The flow becomes substantially three-dimensional that causes the sharp growth of amplitude of oscillations (Fig. 9).

We found that the quaternary state of convection arises at about $Gr = 1.45 \times 10^2$ for $\Delta = 50$ and $Gr \approx 1.5 \times 10^2$ for $\Delta = 75$. According to Fig. 9, the points of bifurcation for this pattern cannot be determined so clear as before, but visual observations of flow support these values.

The experiments have shown that at some conditions flow may undergo one more transition. As the Grashof number exceeds the value $Gr = 1.6 \times 10^2$ for $\Delta = 50$ or $Gr = 1.7 \times 10^2$ for $\Delta = 75$, we fixed the appearance of the longitudinal rolls (or streams) standing between ascending and descending flows.

Variation of the frequency of oscillations nondimensionalized by using time unit h^2/v with the Grashof number Gr is presented in Fig. 10. The black and open squares indicate the results for layers with $\Delta = 50$ and 75 respectively. Some representative results including the power spectra and time series are shown in Fig. 11, where all values are given in the dimension units. The numerical and experimental values of the basic frequency in the dimensionless unit are listed in Table 2.

Fig. 12 presents the singular values spectrum (only five maximal values normalized to the leading value are

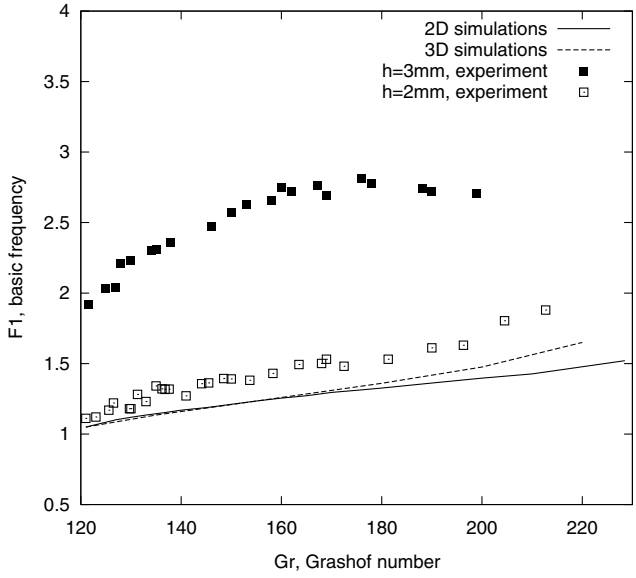

Fig. 10. The variation of frequency of oscillations with the Grashof number. Experimental results for $\Delta = 50$ and 75 are indicated by the black and open squares respectively. Solid and dashed lines indicate the numerical results for two- and three-dimensional convection respectively.

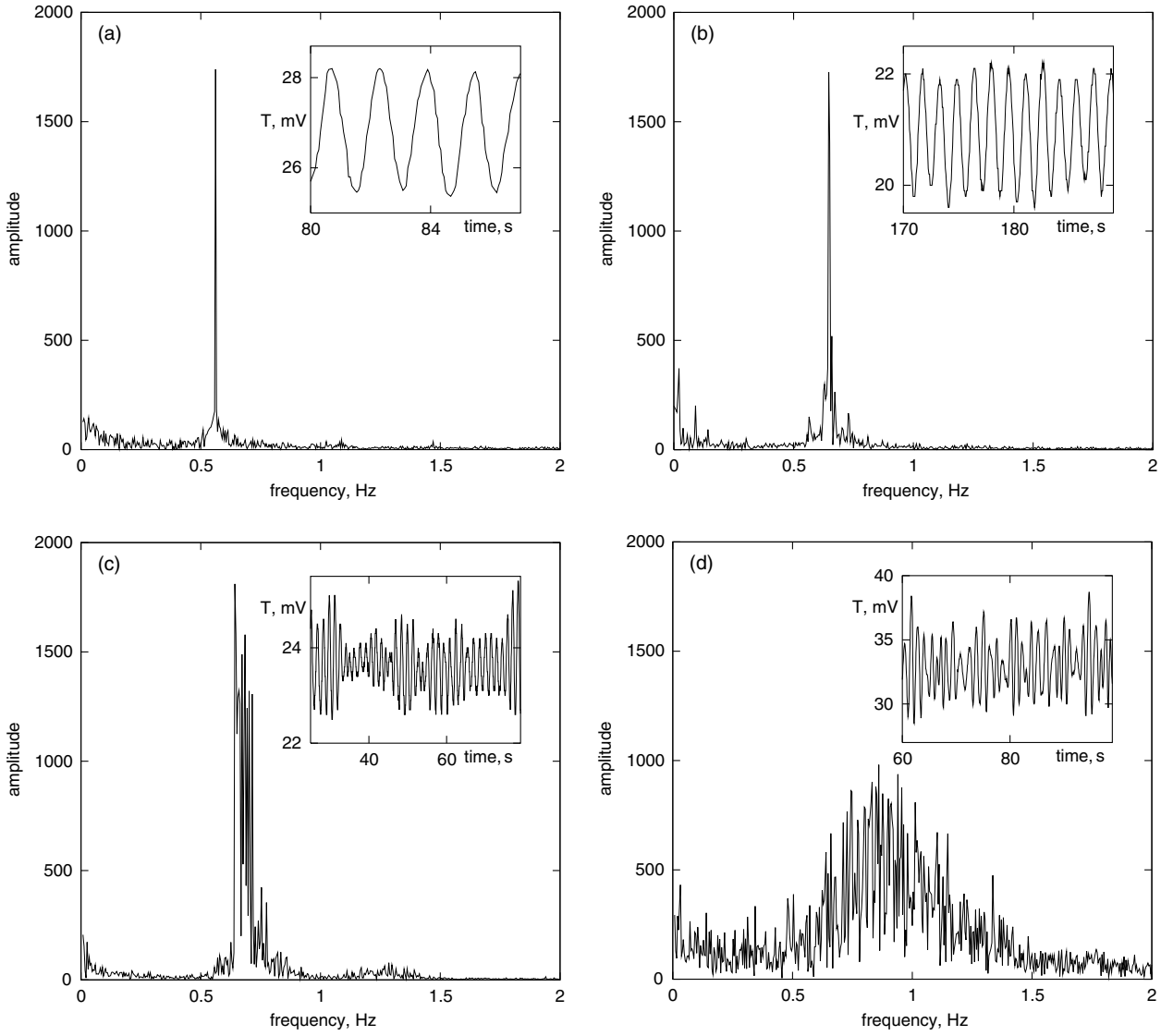

Fig. 11. The power spectra and time series derived from the experimental data for $\Delta = 75$: (a) $Gr = 130$; (b) $Gr = 135$; (c) $Gr = 150$; (d) $Gr = 190$.

Table 2
Values for the basic frequency F_1

Gr	Basic frequency F_1 in dimensionless units			
	2D flows (num.)	3D flows (num.)	$\Delta = 50$ (exp.)	$\Delta = 75$ (exp.)
130	1.11	1.11	2.23	1.18
135	1.19	1.19	2.31	1.34
150	1.24	1.24	2.57	1.39
190	1.34	1.42	2.72	1.61

shown) as a function of the Grashof number Gr for $\Delta = 75$. A singular value, derived within SVD-method, characterizes an intensity of phase motion in the corresponding direction of the reconstructed phase space. Thus, the number of values exceeding the level of noise (indicated in Fig. 12 by horizontal line) gives the dimension of phase space. As it is seen from Fig. 12, the embedding dimension of attractor becomes equal three at $Gr \approx 1.3 \times 10^2$ that can be interpreted as transition from periodic state to more complex behavior. Another crisis of flow occurs at about $Gr \approx 1.7 \times 10^2$, when the dimension of phase space becomes equal four. It is interesting to notice the qualitative similarity of the reconstructed phase portrait (Fig. 13(a)) with the phase dynamics of system obtained numerically (Fig. 13(b)). Both results correspond to $Gr = 135$. The abscissa X_1 and ordinate X_2 in Fig. 13(b) are by the singular eigenvectors giving non-noisy subspace in the embedded space.

5. Flow patterns: simulations versus experiment

Let us discuss how our numerical simulations made for the layer of infinite extent correlate with experimental

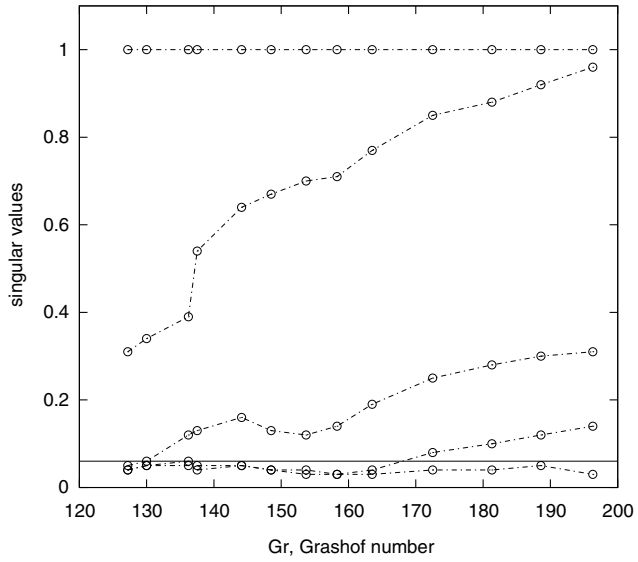

Fig. 12. The variation of five leading singular values σ_i with the Grashof number for attractor reconstructed on the base of the experimental data for the slot $\Delta = 75$. Noise level is indicated by the dashed line.

observations. All the results which we obtained both numerically and experimentally for the flow evolution are listed in Table 1, where the numbers are the critical values of the Grashof number for the onset of a new state, and Table 2 with the values of the principal frequency F_1.

Let us consider in more detail the evolution of flow patterns with the increase of the Grashof number. Note that all photographs, which are discussed below, have been made when the convection cell was illuminated in a scattering light. Bright (dark) areas indicate predominantly the fluid motion parallel (transverse) to the side wall, when the aluminum particles being disk-shaped reflect this light directly to an observer.

It is known from theory that when the Grashof number is small enough, in the system there is a plane-parallel flow, which is described by a cubic profile of velocity and linear profile of temperature (6). Experimental observation for this flow gives the picture, characterizing the uniform distribution of the aluminum particles over cavity (Fig. 14(a)). As it was mentioned before, the theoretical analysis of the stability of a plain-parallel flow with respect to infinitesimal disturbances gives the critical value of the Grashof number $Gr = 115$ for the onset of oscillations (this corresponds to the minimum of neutral curve in Fig. 2). This value is quite close to those $Gr = 1.1 \times 10^2$ ($\Delta = 50$) and $Gr = 1.2 \times 10^2$ ($\Delta = 75$) obtained experimentally. And both the theory (Fig. 7(a)) and experiment (Fig. 14(b), $Gr = 130$) agree on defining the pattern of the secondary flow: this is the system of the two-dimensional transverse rolls standing between downward and upward streams. The intensities of neighboring rolls pulsate periodically in anti-phase. This standing wave is a result of interference of two traveling waves one of which rises and another comes down. The process of the periodic excitation and damping of the transverse rolls could be easily seen visually at an observation of convective cavity from the ends. Such observation of flow through the Plexiglas of heat-exchanger in the scattering light gives the integral picture of the periodic system of bright and dark horizontal stripes (Fig. 14(b)) moving downward or upward depending on the observation plane lying near the cold or hot wall respectively. The similar picture was observed by animation of the velocity field (Fig. 7(a)) obtained numerically.

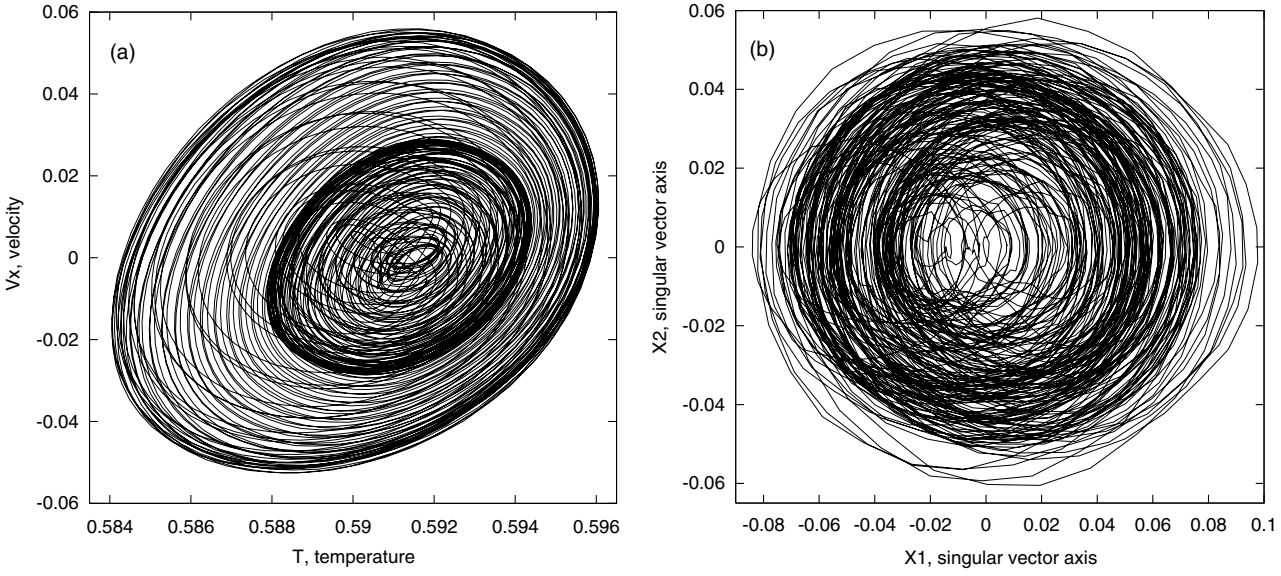

Fig. 13. The phase portrait of the system obtained numerically (a) and reconstructed from the experimental data for $\Delta = 75$ (b). Both pictures correspond to $Gr = 135$.

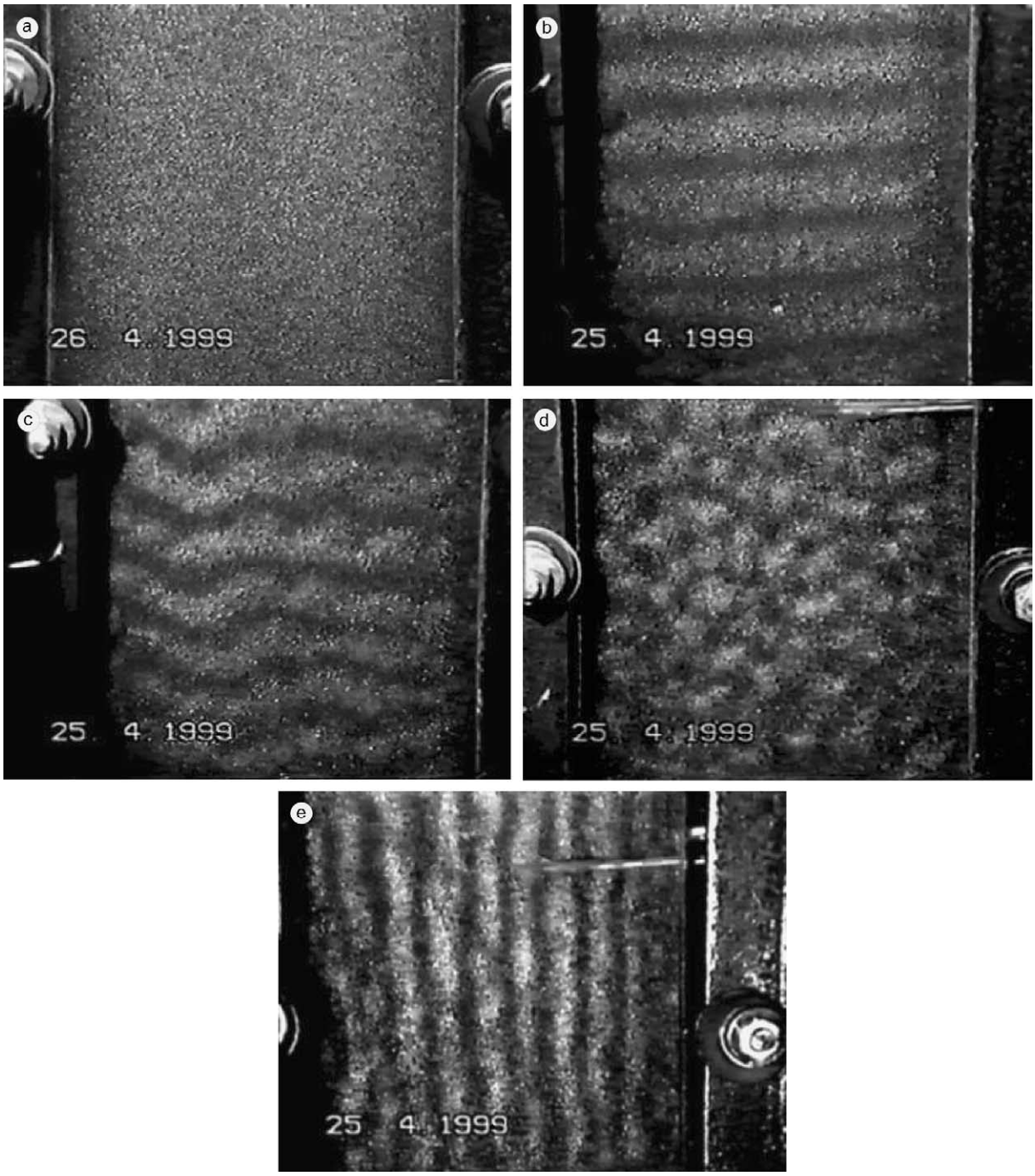

Fig. 14. Photographs of flow patterns for $\Delta = 75$: (a) $Gr = 100$, the plane-parallel flow; (b) $Gr = 130$, the traveling waves, the flow oscillates periodically in time; (c) $Gr = 145$, the wavy traveling waves, the flow oscillates almost quasi-periodically; (d) $Gr = 160$, the cellular pattern, the time dynamics is fully chaotic; (e) $Gr = 190$, the modulated vertical rolls and chaotic oscillations.

As the Grashof number is increased further, the secondary flow becomes unstable to the three-dimensional disturbances. The critical value of Gr we obtained numerically is $Gr = 133$ (for a cell with wave numbers $k_y = \pi/4$, $k_z = \pi/3$). The critical values determined experimentally are $Gr = 1.25 \times 10^2$ for $\Delta = 50$ and $Gr = 1.4 \times 10^2$ for $\Delta = 75$. Both in the numerical simulation (Fig. 7(b), $Gr = 135$) and in the experiment (Fig. 14(c), $Gr = 145$) the instability giving rise to tertiary flow is a wavy instability. It means that the roll pattern becomes wavy in the horizontal direction. The heat exchange between cold and hot streams in the flow intensifies and results in the growth of amplitude of oscillations and the Nusselt number.

Further increase of the Grashof number Gr leads to more influence of the three-dimensional effects on flow

pattern causing the wavy rolls to be pulled apart. This produces the cellular-like pattern shown in Fig. 7(c) ($Gr = 150$) and Fig. 14(d) ($Gr = 160$).

The most intriguing flow pattern forms at about $Gr = 1.6 \times 10^2$ ($\Delta = 50$) or $Gr = 1.7 \times 10^2$ ($\Delta = 75$). A typical photograph of such a flow is shown in Fig. 14(e) for $Gr = 190$. Due to numerical complexity we could not determine the onset of this flow numerically, but observed a similar structure at $Gr = 200$ and larger values of Gr (Fig. 7(d), $Gr = 300$). We found that evolution of the broken rolls leads to the vertical rolls. There are two series of such structure: one standing in ascending flow and another in descending flow. These vertical rolls are not uniform along their axes: the modulation waves travel along them downward in cold flow and upward in hot flow such a way that the fluid elements move on a spiral path.

The comparative analysis of the data obtained numerically and experimentally has shown that there exists qualitative and sometimes even quantitative agreement. It is important to note, that for higher values of the Grashof number the agreement becomes solely qualitative. In our opinion, the problem geometry used in numerical simulations is the main reason for that. It is evident that the theoretical assumption of an infinity of the layer, which permits to consider spatially periodic flows, is a model simplifying the analysis. On the other hand, the experimental setup has a limited vertical extent and consequently finite aspect ratio. In order to permit to the oscillatory disturbances in the opposing streams to grow up to interaction between them, one needs to have the experimental slot sufficiently long. This allows to compare experimental results with those for infinite layer, where such an interaction is assumed a priori. As we noticed in Section 1, the choice of a working fluid is limited to the range $20 \leqslant Pr \leqslant 40$. In our experiments we used the kerosene $Pr = 26$ which applies the condition $\Delta > 50$ on the height of the slot. By analyzing the experimental data listed in Tables 1 and 2, one can conclude that the aspect ratio of cavity has strong influence on the flow, but as the Δ is increased, the results tend to approximate those obtained numerically for infinite layer. Thus, if the cavity with $\Delta = 50$ gives the frequency of oscillations twice as great as theoretical value, then the cavity with $\Delta = 75$ gives the value which is close to the theoretical one (Fig. 9).

6. Summary

Non-linear dynamics and pattern formation of the thermal convection in a tall vertical slot differently heated from the side walls were studied both numerically and experimentally. The kerosene have been chosen as a working fluid, because its Prandtl number $Pr = 26$ is large enough to ensure an onset of traveling waves as primary instability and small enough to prevent an occurrence of boundary layer convection.

In the numerical simulation we have accepted an approximation of infinite layer. The finite-difference and spectral-element methods have been applied to study two- and three-dimensional flows respectively.

In the part of the experimental study, we have used the convection cells with aspect ratio 50 and 75. The stability boundaries have been determined on the base of visual observations, reprocessing of local values of temperature field recorded from the several thermocouples, analysis of the power spectra and amplitude characteristics of oscillations.

We have found that the transition from a plain-parallel cubic profile flow to the convection motions, which are chaotic in time, occurs after a small number of quasi-periodic bifurcations, final destruction of high-dimensional torus (dimension three or four) and appearance of strange attractor. The evolution of flow pattern to space irregularity includes the following sequence of events. In the beginning the plane-parallel flow becomes unstable to pulsating transverse rolls located between ascending and descending flows. As the Grashof number increases, these rolls become wavy and eventually are pulled apart giving rise to cellular-like pattern. Finally, the system evolves to the longitudinal rolls chaotically modulated along their axes.

Thus, the special choice of a working fluid and the taking into account several factors has made it possible for the first time to follow the evolution of the traveling-wave instability with the Grashof number up to values of Gr twice as high as the value of oscillations onset. The comparison of the experimental data with the numerical results for infinite layer has shown a satisfactory agreement between them.

Acknowledgements

The authors wish to thank Prof. B. Roux, Prof. D. Lyubimov and Prof. G. Gershuni (died in 1999) for their useful suggestions. The research described in this publication was made possible in part by Russian Foundation for Basic Research and Administration of Perm Region, Russia, under grant 01-02-96479, and award no. PE-009-0 of the US Civilian Research & Development Foundation for the Independent States of the Former Soviet Union (CRDF).

References

Batchelor, G.K., 1954. Heat transfer by free convection across a closed cavity between vertical boundaries at different temperatures. Quart. Appl. Math. 12, 209–233.

Bergholz, R.F., 1978. Instability of steady natural convection in a vertical fluid layer. J. Fluid Mech. 84, 743–768.

Birikh, R.V., 1966. On small perturbations of a plane parallel flow with a cubic velocity profile. Prikl. Math. Mekh. 30, 356–361.

Birikh, R.V., Gershuni, G.Z., Zhukhovitskii, E.M., Rudakov, R.N., 1972. On the oscillatory instability of plane-parallel convective motion in a vertical channel. Prikl. Math. Mekh. 36, 745–748.

Broomhead, D.S., King, G.P., 1986. Extracting qualitative dynamics from experimental data. Physica D 20, 217–239.

Chait, A., Korpela, S.A., 1989. The secondary flow and its stability for natural convection in a tall vertical enclosure. J. Fluid Mech. 200, 189–216.

Chen, C.F., Thangam, S., 1985. Convective stability of a variable viscosity fluid in a vertical slot. J. Fluid Mech. 161, 161–173.

Chen, F.L., Wu, C.H., 1993. Unsteady convection flows in a vertical slot containing variable viscosity fluids. Int. J. Heat Mass Transfer 36, 4233–4246.

Christov, C.I., Homsy, G.M., 2001. Nonlinear dynamics of two-dimensional convection in a vertically stratified slot with and without gravity modulation. J. Fluid Mech. 430, 335–360.

Clever, R.M., Busse, F.H., 1995. Tertiary and quarternary solutions for convection in a vertical fluid layer heated from the side. Chaos, Solitons Fractals 5, 1795–1803.

Elder, J.W., 1965. Laminar free convection in a vertical slot. J. Fluid Mech. 23, 77–98.

Feudel, U., Jansen, W., Kurths, J., 1993. Tori and chaos in a nonlinear dynamo model for solar activity. Int. J. Bifurcat. Chaos 3, 131–138.

Fischer, P.F., 1989. Spectral element solution of the Navier–Stokes equations on high performance distributed-memory parallel processors. Ph.D. Thesis, Massachusetts Institute of Technology, Massachusetts.

Fujimura, K., Mizushima, J., 1991. Nonlinear equilibrium solutions for traveling waves in free convection between vertical parallel plates. Eur. J. Mech. B. Fluids 10 (suppl. 2), 25–30.

Gershuni, G.Z., 1953. On the stability of plane-parallel convective fluid flow. Zh. Tech. Fiz. 23, 1838–1844.

Gershuni, G.Z., Zhukhovitskii, E.M., 1976. Convective Stability of Incompressible Fluids (D. Louvish, Trans.) Keter Publications, Jerusalem.

Gershuni, G.Z., Zhukhovitskii, E.M., Tarunin, E.L., 1968. Secondary convective steady motions in a plane vertical fluid layer. Mekh. Zhid. Gaza 5, 130–136.

Gershuni, G.Z., Zhukhovitskii, E.M., Sorokin, L.E., Tarunin, E.L., 1974. Secondary convective oscillatory motions in a plane vertical fluid layer. Mekh. Zhid. Gaza 1, 94–101.

Gollub, J.P., Benson, S.V., 1980. Many routes to turbulent convection. J. Fluid Mech. 100, 449–470.

Hart, J.E., 1971. Stability of the flow in a differently heated box. J. Fluid Mech. 36, 1–15.

Jin, Y.Y., Chen, C.H., 1996. Natural convection of high Prandtl number fluids with variable viscosity in a vertical slot. Int. J. Heat Mass Transfer 39, 2663–2670.

Kirdyashkin, A.G., Leontyev, A.I., Mukhina, N.V., 1971. Stability of laminar fluid flow in a vertical layer at natural convection. Mekh. Zhid. Gaza 5, 170–174.

Korpela, S.A., Gozum, D., Baxi, C.B., 1973. On the stability of the conduction regime of natural convection in a vertical slot. Int. J. Heat Mass Transfer 16, 1683–1690.

Lee, Y., Korpela, S.A., 1983. Multicellular natural convection in a vertical slot. J. Fluid Mech. 126, 91–121.

Nagata, M., Busse, F.H., 1983. Three-dimensional tertiary motions in a plane shear layer. J. Fluid Mech. 135, 1–26.

Packard, N.H., Crutchfield, J.P., Farmer, J.D., Shaw, R.S., 1980. Geometry from a time series. Phys. Rev. Lett. 45, 712–715.

Patera, A.T., 1984. Spectral element for fluid dynamics: laminar flow in a channel expansion. J. Comput. Phys. 54, 486–488.

Pazó, D., Sánchez, E., Matías, M.A., 2001. Transition to high-dimensional chaos through quasiperiodic motion. Int. J. Bifurcat. Chaos 11, 2683–2688.

Ruelle, D., Takens, F., 1971. On the nature of turbulence. Commun. Math. Phys. 20, 167–192.

Seki, N., Fukusako, S., Inaba, H., 1978. Visual observation of natural convective flow in a narrow vertical cavity. J. Fluid Mech. 84, 695–704.

Takens, F., 1981. Detecting strange attractors in turbulence. In: Dynamical Systems and Turbulence. In: Rand, D.A., Young, L.S. (Eds.), Lecture Notes in Mathematics, vol. 898. Springer-Verlag, Berlin, pp. 366–381.

Wakitani, S., 1994. Experiments on convective instability of large Prandtl number fluids in a vertical slot. ASME J. Heat Transfer 116, 120–126.

Walden, R.W., Kolodner, P., Passner, A., Surko, C.M., 1984. Nonchaotic Rayleigh–Bénard with four and five incommensurate frequencies. Phys. Rev. Lett. 53, 242–245.